$$(\alpha_S^5 - 1)/z = 67/21 \quad \text{(A.2)}$$

from which the desired M_w dependence of z could be obtained and which seems to be the best approach in the high molecular weight region.

These z values were then inserted into eq 7 of Tanaka[15]

$$h(z) = (1 + 7.16z)^{-2/5} \quad \text{(A.3)}$$

and with this function we eventually calculated $\psi(z)$ and A_2 as a function of M_w.

Appendix 2

To calculate A_2 for short stiff chains, we used a procedure worked out by Yamakawa and Stockmayer.[16] With their eq 119, the function $H(L,d)$ was calculated, where L is the contour length and d the thickness of the chain (=0.88 nm).

With the aid of α_S data, interpolated from experimental data, we can estimate reasonable values for z by use of

$$\alpha_S^5 - \alpha_S^3 = (67/70)Kz \quad \text{(A.4)}$$

where K is given by their eq 83 with eq 85.

Now we were able to calculate the interpenetration function $\psi(\bar{z})$, where $\bar{z}$ is defined as

$$\bar{z} = z/\alpha_S^3 \quad \text{(A.5)}$$

$$Q(L) = 2L^{-5/2}H(L,d) \quad \text{(A.6)}$$

$$\bar{z}h(\bar{z}) = (2Q)^{-1} \ln (1 + 2Qz) \quad \text{(A.7)}$$

$$\psi(\bar{z}) = (\langle S^2\rangle_0/\langle S^2\rangle_{z\theta})^{3/2}\bar{z}h(\bar{z}) \quad \text{(A.8)}$$

$\langle S^2\rangle_{z\theta}/\langle S^2\rangle_0$ is the ratio of the mean square radius of gyration to the Gaussian coil limit value $\langle S^2\rangle_0$ according to eq 22. A_2 is calculated by

$$A_2 = (4\pi^{3/2}N_A\langle S^2\rangle^{3/2}/M^2)\psi(\bar{z}) \quad \text{(A.9)}$$

Registry No. PS (homopolymer), 9003-53-6; neutron, 12586-31-1.

References and Notes

(1) ter Meer, H.-U.; Burchard, W.; Wunderlich, W. *Colloid Polym. Sci.* **1980**, *285*, 675.
(2) Cowie, J. M. G.; Worsfold, D. J. *Trans. Faraday Soc.* **1961**, *57*, 705.
(3) Bantle, S.; Schmidt, M.; Burchard, W. *Macromolecules* **1982**, *15*, 1604.
(4) King, T. A.; Knox, A.; Lee, W. I.; McAdam, J. D. C. *Polymer* **1973**, *14*, 151.
(5) Han, C. C.; McCrackin, F. L. *Polymer* **1979**, *20*, 427.
(6) Jones, G.; Caroline, J. *J. Chem. Phys.* **1979**, *37*, 187.
(7) Bawn, C. E. H.; Wajid, M. A. *J. Polym. Sci.* **1957**, *12*, 109.
(8) Berry, G. C. *J. Chem. Phys.* **1966**, *44*, 4550.
(9) Norisuye, T.; Fujita, H. *Polym. J.* **1982**, *14*, 143.
(10) Yamakawa, H.; Fujii, M. *Macromolecules* **1973**, *6*, 407.
(11) Oseen, C. W. "Hydrodynamik"; Akademische Verlagsgesellschaft: Leipzig, 1927.
(12) Burgers, J. M. "Second Report on Viscosity and Plasticity of the Amsterdam Academy of Sciences"; Nordemann: New York, 1983, Chapter 3.
(13) Hearst, J. E.; Stockmayer, W. H. *J. Chem. Phys.* **1962**, *37*, 1425.
(14) Miyaki, Y.; Einaga, Y.; Fujita, H. *Macromolecules* **1978**, *11*, 1180.
(15) Tanaka, G. *J. Polym. Sci., Polym. Phys. Ed.* **1979**, *17*, 305.
(16) Yamakawa, H.; Stockmayer, W. H. *J. Chem. Phys.* **1972**, *57*, 2843.
(17) Yamakawa, H. "Modern Theory of Polymer Solutions"; Harper and Row: New York, 1971.
(18) Schmidt, M.; Burchard, W. *Macromolecules* **1981**, *14*, 210.
(19) Huber, K. Diploma Thesis, Freiburg, 1982.
(20) Raczek, J. Dissertation, Mainz, 1980.
(21) Strazielle, C.; Benoit, H. *Macromolecules* **1975**, *8*, 203.
(22) Ballard, D. G. H.; Rayner, M. G.; Schelten, J. *Polymer* **1976**, *17*, 349.
(23) Kirste, R. G.; Wild, G. *Makromol. Chem.* **1969**, *121*, 174.
(24) Appelt, B.; Meyerhoff, G. *Macromolecules* **1980**, *13*, 657.
(25) Meyerhoff, G.; Schulz, G. V. *Makromol. Chem.* **1951**, *7*, 294.
(26) Flory, P. J. "Principles of Polymer Chemistry"; Cornell University Press: Ithaca, NY, 1953.
(27) Burchard, W.; Schmidt, M.; Stockmayer, W. H. *Macromolecules* **1980**, *13*, 580, 1265.
(28) Kirkwood, J. G.; Riseman, J. *J. Chem. Phys.* **1948**, *16*, 565.
(29) Daniels, H. E. *Proc. R. Soc. London, Ser. A* **1952**, *63*, 290.
(30) Burchard, W. Habilitationsschrift, Freiburg, 1966.
(31) Benoit, H.; Doty, P. *J. Chem. Phys.* **1953**, *57*, 958.
(32) Mokrys, I. J.; Rigby, D.; Stepto, R. F. T. *Ber. Bunsenges. Phys. Chem.* **1979**, *83*, 446.
(33) Edwards, C. J. C.; Rigby, D.; Stepto, R. F. T. *Macromolecules* **1981**, *14*, 1808.
(34) Bantle, S., unpublished data.
(35) Institut Max von Laue-Paul Langevin, "Neutron Beam Facilities Available for Users", Jan 1981 edition.
(36) Ghosh, R. E. "A Computing Guide for SANS Experiments at the ILL", 1981, GH 29T.
(37) Dandliker, W. B.; Krautt, J. *J. Am. Chem. Soc.* **1956**, *78*, 2380.

(38) A change of the value for A_1 requires a corresponding change of the coefficients C_i in eq 25, which guarantees that the two curve sections of eq 24 and 25 have at $L = \sigma$ the same value and the same derivative. Since, however, in the present treatment eq 25 was not needed, we did not carry out the corresponding alteration.

Detailed Molecular Structure of a Vinyl Polymer Glass

Doros N. Theodorou and Ulrich W. Suter*

Department of Chemical Engineering, Massachusetts Institute of Technology, Cambridge, Massachusetts 02139.

Received November 9, 1984

ABSTRACT: A method is developed for the detailed atomistic modeling of well-relaxed amorphous glassy polymers. Atactic polypropylene at −40 °C is used as an example. The model system is a cube with periodic boundaries, filled with segments from a single "parent" chain. An initial structure is generated by using a modified Markov process, based on rotational isomeric state theory and incorporating long-range interactions. This structure is then "relaxed" by potential energy minimization, using analytical derivatives. Computing time is kept relatively small by stagewise minimization, employing a technique of "blowing up" the atomic radii. Model estimates of the cohesive energy density and the Hildebrand solubility parameter agree very well with experiment. The conformation of the single chains in the relaxed model system closely resembles that of unperturbed chains. Pair distribution functions and bond direction correlation functions show that the predominant structural features are intramolecular and that long-range orientational order is completely absent.

Introduction

An accurate description of glassy polymers in detailed molecular terms is not available to date, and as a result there is no theoretical treatment of deformation and relaxation phenomena in polymeric glasses based on "first principles"; consequently, phenomenological concepts[1]

0024-9297/85/2218-1467$01.50/0

which defy precise definition, such as "free volume", must be invoked. Chain packing in the amorphous bulk has been studied extensively, and newer experimental data, especially from neutron scattering, strongly suggest[2-5] that the chain macromolecules assume essentially unperturbed random coil conformations, in the "equilibrium" melt and even in well-relaxed glasses. Flory[6] suggested this decades ago, but the complete absence of long-range orientational correlation, implied by the random coil model, is nevertheless not universally accepted.[7] The objective of this work is the development of a quantitative computer model of molecular structure in an amorphous polymer (atactic polypropylene) below its glass formation temperature. This will serve as a point of departure for the prediction of structural and thermodynamic properties of the bulk polymer. The primary limitations encountered in this endeavor are the computing resources currently available; we have nevertheless tried to make the structural model as realistic as possible.

Previous Work

Theoretical investigations of structure in the amorphous polymeric bulk have typically involved Monte Carlo simulations of the topology of multichain systems. Polymer molecules are frequently modeled as self-avoiding random walks on a discrete lattice of sites with cyclic boundary conditions. Primitive cubic[8-11] lattices, as well as more realistic "diamond" lattices,[12,13] or even regular two-dimensional lattices of various coordination numbers[14] have been used. Various sampling methods have been devised to limit sample attrition, which is severe at high densities. The objective is usually investigation of the effects of the volume fraction and the length of the chains on conformation-related quantities such as the mean squared end-to-end distance, $\langle r^2 \rangle$, and the mean squared radius of gyration, $\langle s^2 \rangle$. A general conclusion is that $\langle r^2 \rangle$, $\langle s^2 \rangle$, and $\partial \ln \langle r^2 \rangle / \partial \ln n$ fall as the volume fraction increases toward unity, approaching the values characteristic of an unperturbed random walk. Residual differences between some Monte Carlo models and Flory's "unperturbed random coil theory" are probably partly due to the simplifying assumptions and sampling techniques used.

A somewhat more sophisticated Monte Carlo model for a "liquid" has been published by Bishop et al.[15] Chains are pictured as freely jointed strings of beads, which interact with each other through a Lennard-Jones potential and which are connected by bonds of finite extensibility. A reptation algorithm is used to sample configuration space.

Considerably more realistic is a computer model of the molecular arrangement in a polymer *liquid*, consisting of short linear polymethylene chains, advanced by Vacatello et al.[16] The system modeled is a cubic cell with periodic boundaries, of edge length 30.4 Å and filled with 31 triacontane chains. The packing corresponds to the experimental density of the paraffinic liquid. Chains are modeled as sequences of methylene units connected by bonds of fixed length, and bond angles are given tetrahedral values. The chains are initially "grown in situ" in a lattice, starting from randomly oriented trimethylene units. The system is subsequently "equilibrated" by a Monte Carlo procedure which resembles reptation but allows for continuous variation of bond angles. Hence, the final model is not a lattice model. The methylene–methylene nonbonded interaction potential is changed during "equilibration" to save computer time. The structure is evaluated only during the latter stages of equilibration so that the number of microstates sampled is much smaller than in an ordinary Metropolis Monte Carlo procedure. Predicted X-ray scattering curves agree satisfactorily with experimental data, and characteristic quantities of the model chains indicate an essentially unperturbed conformation.

A molecular dynamics approach to the problem of modeling the structure of amorphous polymers has been introduced by Weber and Helfand.[17] Their system is a "liquid" periodic polyethylene chain in a box of edge length 18.2 Å, containing 200 carbon centers, at 425 K. Structural and dynamic information is accumulated from a run simulating the temporal evolution of the system.

Polyethylene seems to be the only polymer chain on which realistic modeling of the structure of the amorphous bulk has been attempted, and these attempts have been restricted to the liquid state. No computer simulation has ever been performed at densities corresponding to a glass.

Molecular Model Parameters

The selected polymer system is atactic polypropylene at 1 atm and −40 °C, i.e., ca. 20 °C below its glass formation temperature, T_g, of ca. −18 °C.[18-21] At this temperature interval below T_g polymeric glasses are solids for all practical purposes;[22] characteristic times for volume relaxation are of the order of years,[22] and molecular motion consists predominantly of solidlike vibrations of atoms around their average equilibrium positions.[23] The density of a well-relaxed polypropylene glass at −40 °C is[20] ca. 0.892 g cm^{-3}.

Polypropylene was chosen since the simple alkane structure permits the use of simple and well-known expressions for the potential energy of interatomic interactions. Also, the atactic form ensured complete absence of crystallinity. In addition, atactic samples of well-defined configurational statistics can be readily obtained.[21]

Our molecular model follows Cohen and Turnbull's[24] concept of glasses being in a state of frozen-in liquid disorder. It rests on the following four assumptions:

A. The model does not incorporate thermal motion; i.e., it is static. Temperature enters only indirectly, through specification of the density.

B. The polymer is represented as an ensemble of microscopic structures. All parts of a microstructure (atoms, groups, and bonds) satisfy the requirements of detailed mechanical equilibrium.

C. Bond lengths and bond angles are fixed. Molecular movements occur exclusively through rotation around skeletal bonds.

D. Backbone carbon atoms and pendant hydrogen atoms are treated explicitly, but methyl groups are lumped into single "quasi-atoms" of appropriate size.

Assumption A reflects the fact that we focus on the atomic positions of static mechanical equilibrium, as one would do in a crystal. By thus stripping the system of its thermal motion (and introducing only a "mean field" temperature), we achieve a dramatic reduction in the degrees of freedom. Alternatively, a full simulation of the system, in both configuration and momentum space, could be attempted by molecular dynamics; with the present computational capabilities, however, dynamic simulations could only cover an exceedingly short time span, and one would not depart significantly from the vicinity of the initial guess structure. Also, static simulations in the spirit of the one presented here have been performed for metallic glasses with very satisfactory results.[25,26]

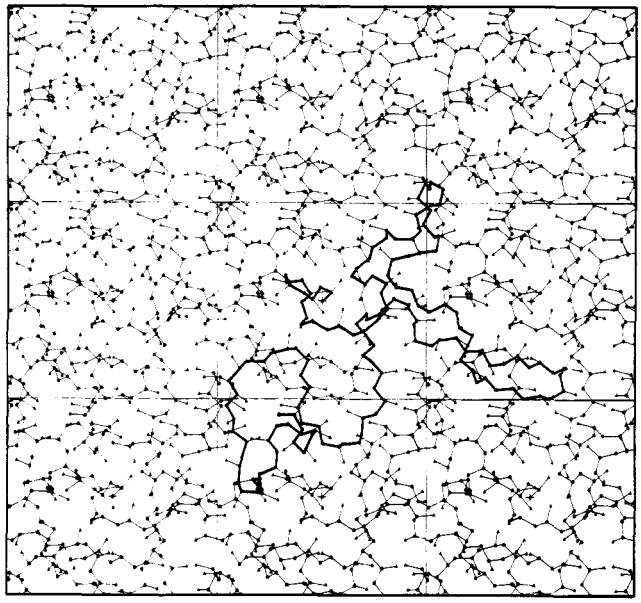

Figure 1. Model structure in the cube (center) and eight of its neighboring images, projected on the xy plane. The parent chain is traced with a bold line, the image chains are drawn as thin lines. All carbon atoms are indicated; hydrogen atoms are omitted for clarity.

Assumption B, i.e., the requirement that the modeled microstates be in mechanical equilibrium (at local minima of the total potential energy), should not be interpreted as implying thermodynamic equilibrium (a minimum of the Helmholtz energy would be required for this). Each structure generated in our investigation is only one microstate, and the microstates do not comprise an equilibrium ensemble.

Assumptions C and D are merely computational expedients.

The model system is a cube of glassy atactic polypropylene with three-dimensional periodic boundaries, filled with chain segments at a density corresponding to the experimental value for the polymer. The entire contents of the cube are formed from a single "parent chain" of the constitution R–CHR(CH_2CHR)$_{x-1}$–R, where R is a methyl group. The cube can thus be considered as part of an infinite medium, consisting of displaced images of the same chain (see Figure 1). Computer time considerations limited the size of our parent chain to $x = 76$ monomeric units. The cube has then edges 18.15 Å long. A total of $6x - 1 = 455$ interacting atoms and groups are present in the cube.

With the simplifications introduced above, the state of the system is completely defined if one specifies (i) the tacticity of the parent chain, (ii) three "Eulerian angles", ψ_1, ψ_2, and ψ_3, describing the orientation of the parent chain with respect to the frame of reference of the cube, and (iii) the $2x - 2$ rotation angles ϕ_i of all skeletal bonds of the parent chain but the first and last. The vector $[\psi_1, \psi_2, \psi_3, \phi_2, \phi_3, ..., \phi_{2x-1}]$ is the "vector of degrees of freedom" of our system. Notice that the coordinates of the chain start do not constitute degrees of freedom, because the system structure is invariant under translation of the cube along its edge vectors. On the contrary, Eulerian angles affect the periodic continuation and thus are degrees of freedom, contrary to what would happen in the case of an isolated single chain.

The geometrical parameters of the chain employed in this simulation have been used in earlier calculations;[27] they are listed in Table I. Nonbonded interatomic interactions are modeled by a finite range modification of

Table I
Geometry and Potential Parameter Values[22,27]

	Bond Lengths (Å)
C–C	$l = 1.53$
C–H	$l_H = 1.10$
C–R	$l_R = 1.53$
	Bond Angle Supplements (degrees)
intradyad C–C–C	$\theta' = 66$
interdyad C–C–C	$\theta'' = 68$
intradyad C–C–H	$\theta'_H = 71$
interdyad C–C–R	$\theta''_R = 68$
interdyad C–C–H	$\theta''_H = 73.2 = \cos^{-1}[\{(1 - 2\cos\theta'')/3\}^{1/2}]$

i	atom or group	r_i°,[a] Å	α_i,[b] Å^3	$N_{e,i}$[c]
1	H	1.3	0.42	0.9
2	C	1.8	0.93	5.0
3	R(methyl)	2.0	1.77	7.0

[a] van der Waals radius. [b] Polarizability. [c] Effective number of electrons.

the Lennard-Jones potential function in which the potential "tail" is substituted by a quintic spline:

$$U^{NB}(r) = U^{LJ}(r) \equiv 4\epsilon\left\{\left(\frac{\sigma}{r}\right)^{12} - \left(\frac{\sigma}{r}\right)^{6}\right\}, \qquad r < R_1 \tag{1a}$$

$$U^{NB}(r) = \epsilon(1-\xi)^3\left\{\frac{U_1^{LJ}}{\epsilon} + \left(3\frac{U_1^{LJ}}{\epsilon} + \Delta\frac{U'_1{}^{LJ}}{\epsilon/\sigma}\right)\xi + \left(6\frac{U_1^{LJ}}{\epsilon} + 3\Delta\frac{U'_1{}^{LJ}}{\epsilon/\sigma} + \frac{\Delta^2}{2}\frac{U''_1{}^{LJ}}{\epsilon/\sigma^2}\right)\xi^2\right\}, \qquad R_1 < r < R \tag{1b}$$

$$U^{NB}(r) = 0, \qquad R < r \tag{1c}$$

where U_1^{LJ}, $U'_1{}^{LJ}$, and $U''_1{}^{LJ}$ stand for the value, the first derivative, and the second derivative of the Lennard-Jones function at the junction point $r = R_1$, $\Delta = (R - R_1)/\sigma$, and $\xi = (r - R_1)/(R - R_1) = (r/\sigma - R_1/\sigma)/\Delta$. Expression 1 is designed so that the functions U^{NB}, dU^{NB}/dr, and d^2U^{NB}/dr^2 are continuous in the entire range of r and assume values of zero at $r > R$.

In the following calculations two versions of the nonbonded potential energy function $U^{NB}(r)$ from eq 1 are employed: (i) the *full potential*, with $R_1 = 1.45\sigma$ and $R = 2.30\sigma$, which reproduces the shape of the Lennard-Jones curve ($U^{LJ}(r)$) very accurately, and (ii) a cruder, purely repulsive approximation to the Lennard-Jones function, which we refer to in the following as the *soft-sphere potential* and which is obtained from eq 1 by employing the parameter values $R_1 = 0.94\sigma$ and $R = 1.04\sigma$. The parameters σ and ϵ were calculated[22,27] from literature values for atomic polarizabilities, effective numbers of electrons, and van der Waals radii, all listed in Table I.

An intrinsic rotational potential, associated with skeletal bond angle torsion, is modeled by the standard expression

$$U_\phi(\phi) = \frac{k_\phi}{2}(1 - \cos 3\phi) \tag{2}$$

with a barrier height of $k_\phi \approx 2.8$ kcal/mol.

It must be emphasized that the expressions for the potential energies contain no adjustable parameters. This allows for a true test of the predictive power of our model.

Generation of a Model Structure

A model structure that satisfies the conditions of detailed mechanical equilibrium (see assumption B above)

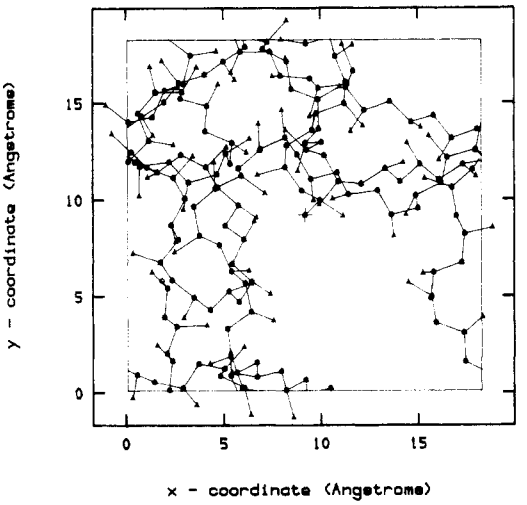

Figure 2. xy projection of an initial-guess structure generated from an "unperturbed" parent chain. Skeletal carbon atoms are shown as circles, methyl carbons are indicated as triangles, and hydrogen atoms are omitted for clarity.

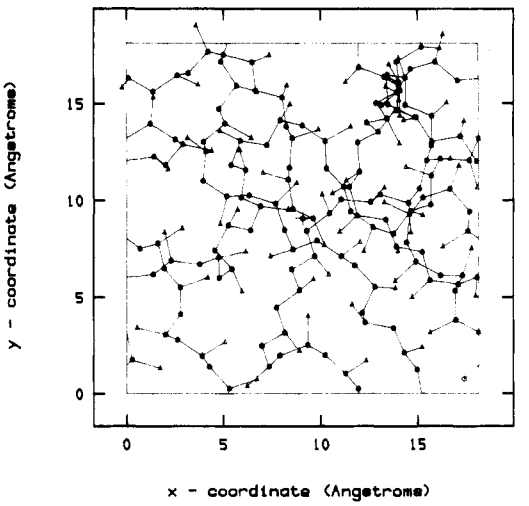

Figure 3. xy projection of an initial-guess structure generated by the "hybrid scheme", eq 3, incorporating long-range interactions. See also legend for Figure 2.

can only be obtained by an iterative process that starts with an appropriately chosen initial guess. Hence, two stages in the evolution of a realistic model structure can be identified: (i) the creation of an initial guess structure, and (ii) the "relaxation" of this structure to a state of minimal potential energy.

Initial Guess. Accepting the view that glasses are in a state of frozen-in liquid disorder also implies that the conformational statistics of the chains are not too different from those of unperturbed macromolecules.

A satisfactory initial guess could be obtained by "random" generation of an unperturbed parent chain and subsequent use of this chain to fill our cube to the correct density. Monte Carlo generation of single unperturbed chains involves the generation of (i) a chain configuration, i.e., a dyad tacticity sequence (in equilibrium atactic polypropylene the configuration statistics are almost Bernoullian,[21] with a fraction of meso dyads equal to $f_m \simeq 0.48$[21,27]), and (ii) a chain conformation, i.e., a sequence of rotation angles. The conformational statistics of unperturbed chains are well described by the rotational isomeric state theory[28,29] (RIS theory). This theory provides us with a priori probabilities $p_{\xi;i}$ (bond i in state ξ) and conditional probabilities $q_{\zeta\xi;i}$ (bond i in state ξ, given bond $i-1$ in state ζ) for all bonds in the chain. The probabilities $p_{\xi;2}$ and $q_{\zeta\xi;i}$ ($3 \le i \le 2x-1$) define an "equivalent Markov process" for the Monte Carlo generation of correctly weighed unperturbed chain conformations. For polypropylene we use the five-state model.[27]

If we try to fill our cube with unperturbed chains, generated with the scheme described above, we discover that the structures obtained are characterized by excessively high energies (order of 10^{12}–10^{15} kcal/mol) and by a very nonuniform spatial distribution of segments (see Figure 2). The reason for this is that the generation procedure incorporates no information about long-range interactions, which are severe at these densities (this does not contradict the "random coil" hypothesis; chains in the bulk are *on the average* similar to chains under Θ-conditions, but this does not mean that *any* Θ-chain can generate an appropriate space-filling model of the polymer under arbitrary periodic conditions). Hence, long-range interactions must be accounted for in order to obtain a realistic initial guess. To do this, we developed the following scheme: (i) We choose the Eulerian angles (ψ_1, ψ_2, and ψ_3) arbitrarily and generate the chain in a bond-by-bond fashion in the cube, observing periodic boundary conditions wherever a bond–border intersection occurs. At each step of the conformation generation we modify the rotational isomeric state conditional probabilities using the formula

$$q'_{\zeta\xi;i} = q_{\zeta\xi;i} \frac{\exp\left[-\dfrac{\Delta U_{\xi;i}^{\mathrm{LR}}}{RT}\right]}{\sum_{\xi'} q_{\zeta\xi';i} \exp\left[-\dfrac{\Delta U_{\xi';i}^{\mathrm{LR}}}{RT}\right]} \tag{3}$$

where $\Delta U_{\xi;i}^{\mathrm{LR}}$ is the increase in long-range interaction energy upon addition to the cube of the skeletal carbon $i+1$ and the substituents of carbon i, if bond i is assigned the rotational state ξ. By "long-range interactions" we mean nonbonded interactions between centers that are five or more bonds apart. Flory's convention[28] is used for the indexing of atoms.

The scheme proposed in eq 3 correctly blends short-range interaction energy (implicitly contained in an exponential form within the $q_{\zeta\xi;i}$ of the RIS model) with long-range interaction energy; i.e., it is a factorization of the full conformation partition function of the system into short- and long-range terms, a pair of terms assigned to each bond. Note, however, that the rotational isomeric state treatment of short-range interactions is truly bidirectional,[28] while the treatment of long-range interactions is only unidirectional since we cannot anticipate overlaps with segments to be generated in the future.

Using the modified conditional probabilities $q'_{\zeta\xi;i}$ we can generate initial guesses which do not depart much from the "random coil hypothesis", have a rather uniform spatial segment distribution, and are of relatively low energy (order of 10^6–10^8 kcal/mol). Thus, the hybrid scheme (3) satisfactorily solves the problem of obtaining a good initial guess (Figure 3).

Relaxation to Mechanical Equilibrium. Each initial guess structure is subjected to a straightforward total potential energy minimization, to reach a microscopic structure that satisfies the conditions of detailed mechanical equilibrium. The total potential energy is the sum of all bond intrinsic rotational potentials and all nonbonded interaction potentials, computed according to the minimum image convention,[30] and the structures in mechanical equilibrium are defined by minima of the total potential energy with respect to the $2x+1$ (= 153) degrees

Table II
Typical Evolution of a Computer Relaxation[a]

potential	starting structure: objective function, kcal/mol	starting structure: gradient norm, kcal/(mol K)	ending structure: objective function, kcal/mol	ending structure: gradient norm, kcal/(mol K)	iterations	function eval	CPU time per function eval, s	CPU time, h
soft spheres, half-radii	0.202×10^3	0.409×10^4	0.798×10^{-19}	0.123×10^{-10}	71	179	4.0	0.20
soft spheres, full radii	0.241×10^5	0.284×10^5	408.272	0.201×10^{-5}	1142	2297	6.8	4.34
full potential	112.508	10.840	108.283	0.790×10^{-6}	279	619	77	13.24

[a] Initial guess: Generated by modified rotational isomeric state scheme (3), $x = 76$, $f_m = 0.480$, $T = 298$ K, chain start at center of cube, $\psi_1 = \psi_2 = \psi_3 = 45°$, total potential energy = 0.111×10^7 kcal/mol. Machine: MIT Honeywell DPS 8/70, operating under MULTICS (approximately equivalent in computational power to a VAX 780); all calculations were made in 8-byte precision.

of freedom $\psi_1, \psi_2, \psi_3, \phi_2, \phi_3, ..., \phi_{2x-1}$. Because of its high dimensionality and nonlinearity the relaxation problem demands a very carefully planned method of attack.

Some key elements of computational strategy employed are described in the following:

A. The $2x + 1$ Eulerian and rotation angles were directly used as variables in an unconstrained minimization problem. A formulation in terms of the individual atom coordinates would involve almost nine times as many variables and would convert the problem to a constrained minimization, which is computationally much harder.

B. Analytical expressions were derived for the total potential energy U, and its first and second derivatives with respect to the microscopic degrees of freedom, with proper consideration of the periodic boundary conditions (see Appendix 1). Observe that, with the potential expressions used, the objective function U, its gradient, and the Hessian matrix of second derivatives are all continuous functions of the degrees of freedom. This ensures a well-behaved minimization.

C. The quasi-Newton matrix-updating algorithm of Broyden, Fletcher, Goldfarb, and Shanno[31,32] was implemented. The optimization routine employs our analytically calculated gradient, an aspect crucial to the success of the method. Use of a finite-difference estimation scheme for the derivatives would not only be numerically inaccurate but also be orders of magnitude more demanding in computation time.[33]

D. The computation time for an energy and gradient evaluation increases steeply with the interatomic potential range (see Table II). Therefore, we employed a three-stage optimization strategy, a different form of the total energy function being used at each step:

Step 1: *Soft-sphere potential* (see above); atomic radii (i.e., Lennard-Jones σ's) of half their actual size; no rotational barriers.

Step 2: *Soft-sphere potential*; radii of actual size; full rotational barriers.

Step 3: *Full potential* (see above); radii of actual size, full rotational barriers.

This makes the system at first "feel" and alleviate only the most severe repulsive interactions, while keeping computation time small. The second step absorbs the bulk of the optimization iterations. In the final stage the attractive part of the potential is "switched on", and the final minimum is reached.

Using the optimization procedure described above we were able to obtain minimum-energy structures characterized by a Euclidean norm of the gradient smaller than 10^{-6} kcal/(mol K). The exact Hessian, calculated for the "final" structures is always positive definite, indicating true minima. A typical computer relaxation history is given in Table II. A three-dimensional view of an equilibrium structure is shown in Figure 4.

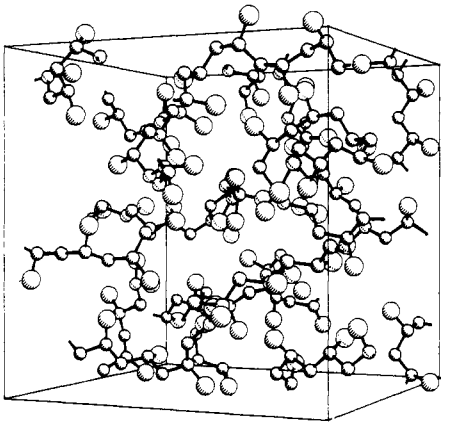

Figure 4. "Relaxed" model structure in detailed mechanical equilibrium. The small spheres denote skeletal carbon atoms, the large spheres indicate methyl groups, and hydrogen atoms have been omitted for clarity.

Results

Fifteen model structures were obtained by the method described above. This ensemble of structures provides us with detailed information, which is analyzed below.

Cohesive Energy Density and Solubility Parameter. The total potential energy of the 15 model structures, computed according to eq A.11 falls in the range (average (±standard deviation))

$$U = 113\ (\pm 20)\ \frac{\text{kcal}}{\text{mol of structures}}$$

However, we have omitted the tails of the nonbonded interaction energy functions. We therefore compute a "tail correction" to the potential energy by

$$\Delta U_{\text{tails}} = \frac{1}{2}\sum_{\alpha=1}^{3} N_\alpha \sum_{\beta=1}^{3} \rho_\beta \Big[4\pi \int_{R_{1,\alpha\beta}}^{R_{\alpha\beta}} g_{\alpha\beta}(r) \times [U_{\alpha\beta}^{\text{LJ}}(r) - U_{\alpha\beta}^{\text{NB}}(r)] r^2\, dr + 4\pi \int_{R_{\alpha\beta}}^{\infty} g_{\alpha\beta}(r) U_{\alpha\beta}^{\text{LJ}} r^2\, dr \Big] \quad (4)$$

where N_α and ρ_α stand for total number and number density of groups belonging to species α in the cube, summation indices 1, 2, and 3 stand for H, C, and R, respectively, $g_{\alpha\beta}$ is the pair distribution function for the species pair $\alpha\beta$ (see below), and all other symbols have been introduced above.

We evaluated expression 4 using the group pair distribution functions discussed in the last section of this paper for distances $r \leq 10$ Å, and assuming $g_{\alpha\beta}(r) = 1$ for $r \geq 10$ Å $\forall$ (α,β). The result is

$$\Delta U_{\text{tails}} = -85\ \frac{\text{kcal}}{\text{mol of structures}}$$

so that

$$U_{tot} = U + \Delta U_{tails} = 28\ (\pm 20)\ \frac{\text{kcal}}{\text{mol of structures}}$$

The contribution of the intrinsic rotational potential to U_{tot} is

$$\sum_{i=2}^{2x-1} U_\phi(\phi_i) = 104\ (\pm 11)\ \frac{\text{kcal}}{\text{mol of structures}}$$

and the rest is due to (predominantly attractive) nonbonded interatomic interactions.

Cohesive energy can be obtained by comparing U_{tot} with the corresponding energy for the isolated parent chain. Cohesive energy is defined[23] as "the increase in internal energy per mole of substance if all intermolecular forces are eliminated". In our model systems each chain is surrounded by other chains, which are simply displaced images of itself. The cohesive energy E_{coh} is the energy of interaction between these images. Each parent chain contains the same amount of matter as a model cube of the bulk polymer, and an estimate of E_{coh} can thus be obtained as the ensemble average of the difference

$$E_{coh} = U_{tot,\,parent} - U_{tot} \tag{5}$$

Hildebrand's solubility parameter is simply the square root of the cohesive energy density

$$\delta = (E_{coh}/V)^{1/2}\ (\text{J/cm}^3)^{1/2} \tag{6}$$

The total potential energy $U_{tot,\,parent}$ of each isolated parent chain was computed by using the *full* Lennard-Jones function to describe nonbonded interatomic interactions and including the intrinsic rotational potential; the energy U_{tot} of the cube formed from the parent chain was subsequently subtracted from $U_{tot,\,parent}$. The resulting difference, based on all 15 structures, is (mean (±standard deviation))

$$E_{coh} = 174\ (\pm 20)\ \frac{\text{kcal}}{\text{mol of structures}} = 227\ (\pm 26)\ \frac{\text{kJ}}{\text{kg of polymer}}$$

whence the cohesive energy density is

$$E_{coh}/V = 2.0\ (\pm 0.2) \times 10^8\ \text{J/m}^3$$

and the theoretical estimate of Hildebrand's solubility parameter is thus

$$\delta = (E_{coh}/V)^{1/2} = 14.2\ (\pm 0.8)\ (\text{J/cm}^3)^{1/2}$$

Experimental values[23] for the solubility parameter (and for the cohesive energy density) are available for polypropylene of unspecified tacticity and probably refer to the commercial isotactic form. Comparison of atactic and isotactic samples suggests that the solubility parameter for the atactic polymer is somewhat lower than the reported one[23] of

$$\delta_{exptl} = 16.8\ (\text{J/cm}^3)^{1/2}$$

corresponding to a cohesive energy density of

$$(E_{coh}/V)_{exptl} = 2.82 \times 10^8\ \text{J/m}^3$$

In light of this agreement between the theoretical prediction and experiment is excellent. This agreement indicates that the atomistic model structures are *realistic*, and we proceed to investigate their microscopic characteristics.

Conformation of the Individual Chains in the Bulk. As a measure of orientational correlation between bonds we use the "bond direction correlation function", or "order parameter", S, defined by[16,17,34]

$$S = \frac{1}{2}[3\langle \cos^2 \theta \rangle - 1] \tag{7}$$

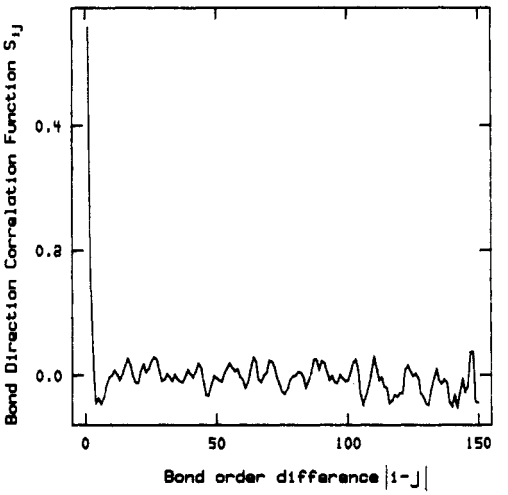

Figure 5. Average bond direction correlation function S_{ij} between skeletal chords in the 15 parent chains vs. the index difference $|i - j|$. See text for details.

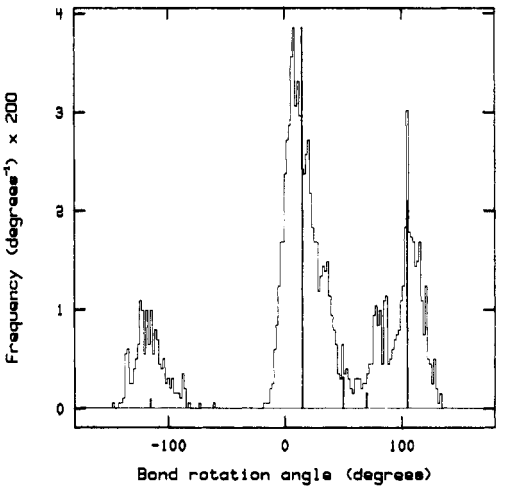

Figure 6. Distribution of torsion angles in the 15 "relaxed" model systems. The corresponding RIS values are given as relative probabilities (bold vertical lines).

where θ is the angle between two skeletal bond chords of the chain (chord i is the vector connecting the midpoints of the skeletal bonds flanking carbon atom i). We denote with S_{ij} that order parameter that is obtained by taking the average in eq 7 over all chord pairs with given index difference $|i - j|$ and over all 15 structures, i.e., by averaging over the squared cosine of the angle between all chords separated by a fixed number of bonds.

Figure 5 shows S_{ij} as a function of $|i - j|$. The strong directional correlation between neighboring chords for very small values of $|i - j|$ vanishes rapidly with increasing distance along the chain. The absence of any long-range correlation effects indicates that the procedure used to generate the structures investigated here indeed leads to parent chains that are "random coils".

To what extent, however, do these chains resemble *unperturbed* random coils? The distribution of rotation angles in the 15 model systems is depicted in Figure 6. The corresponding distribution for unperturbed chains as predicted by the RIS model[27] was obtained as follows: We generated 100 Bernoullian configurations with $x = 76$ and $f_m = 0.48$; we then computed the a priori probabilities of each RIS state using a generator matrix technique[29] and averaged them over all configurations. The a priori probabilities thus obtained appear as "Dirac pulses" in Figure 6 (bold lines); the pulse heights are proportional

Table III
Model System Bond Angle Distribution Compared to Rotational Isomeric State Model Predictions for Unperturbed Chains

state	ϕ interval, deg	state freq obtained from 15 model systems	state a priori probability from RIS model
$\bar{g}$	$-148 < \phi < -60$	0.128 ± 0.039	0.0137 ± 0.0002
t	$-18 < \phi < 30$	0.444 ± 0.055	0.5939 ± 0.0028
t*	$30 < \phi < 59$	0.110 ± 0.026	0.0474 ± 0.0013
g*	$59 < \phi < 89$	0.086 ± 0.022	0.0225 ± 0.0002
g	$89 < \phi < 135$	0.230 ± 0.038	0.3224 ± 0.0016

Table IV
Shape and Size Characteristics of Parent Chains[a]

measure	av value from 15 parent chains	RIS value
$\langle r^2\rangle^{1/2}$, Å	40.12 ± 3.18	47.00 ± 0.10[b]
$\langle s^2\rangle^{1/2}$, Å	17.20 ± 1.06	18.76 ± 0.05[b]
$\langle r^2\rangle/\langle s^2\rangle$	5.44 ± 1.09	6.28 ± 0.04[b]
$\langle\overline{X^2}\rangle/\langle\overline{Z^2}\rangle$	15.24 ± 2.55	14.84 ± 0.25[c]
$\langle\overline{Y^2}\rangle/\langle\overline{Z^2}\rangle$	3.01 ± 0.47	3.13 ± 0.05[c]
$\langle b\rangle/\langle s^2\rangle$	0.687 ± 0.141	0.674 ± 0.013[c]
$\langle c\rangle/\langle s^2\rangle$	0.104 ± 0.093	0.112 ± 0.002[c]
$\langle\kappa^2\rangle$	0.444 ± 0.057	0.431 ± 0.004[c]

[a] Mean values ± standard deviation of the mean. [b] By exact generator matrix method. [c] By Monte Carlo estimation; see text.

to the state probabilities. We observe that rotation angles in our bulk model system concentrate in two major peaks, corresponding to the t and g rotational isomeric states. In addition, one can discern three smaller peaks near the locations of the t*, g*, and $\bar{g}$ states. Thus, qualitative agreement between the angle distribution in the bulk and the RIS prediction is very good. A quantitative comparison was made by division of the torsion angle range into five intervals, each corresponding to a rotational state, and by integrating the rotation angle distribution to obtain the probabilities that ϕ lie in each of these intervals. These probabilities are given, together with the RIS probabilities, in Table III. Although the relative population of the major states in the bulk structures (t/g = 1.93) is very close to that from the RIS model (t/g = 1.84), we observe that the states of lesser population, and in particular $\bar{g}$, are considerably more frequent in the bulk. (The enhancement of the $\bar{g}$ state is also evident from Figure 6.) This indicates that the parent chains are richer in the more compact conformations, and one would expect them to appear somewhat "collapsed" in comparison to unperturbed chains. These conformational differences might be due to the initial guess generation procedure, in which consideration of long-range interactions causes the parent chain conformation probabilities to depart from the RIS values. During the subsequent minimization a large proportion (approximately 36%) of the skeletal bonds "flips" (i.e., changes state), and these flips tend to restore the bond angle distribution toward the RIS values (the fully relaxed structures still show some differences from the state populations in a RIS model, however).

The size of the parent chain was assessed by the ensemble-averaged end-to-end distance $\langle r^2\rangle^{1/2}$ and radius of gyration $\langle s^2\rangle^{1/2}$, displayed in Table IV. The corresponding unperturbed chain values, computed by exact generator matrix methods from 100 Bernoullian configurations with $x = 76$ and $f_m = 0.48$ (see above) are also shown in Table IV. The average expansion factor of our parent chains, calculated from $\langle r^2\rangle^{1/2}$, is 0.85 ± 0.07. The calculation of $\langle s^2\rangle^{1/2}$, however indicates an expansion coefficient of 0.92 ± 0.06; since this value is based on a larger statistical sample than the end-to-end distance (all skeletal carbon

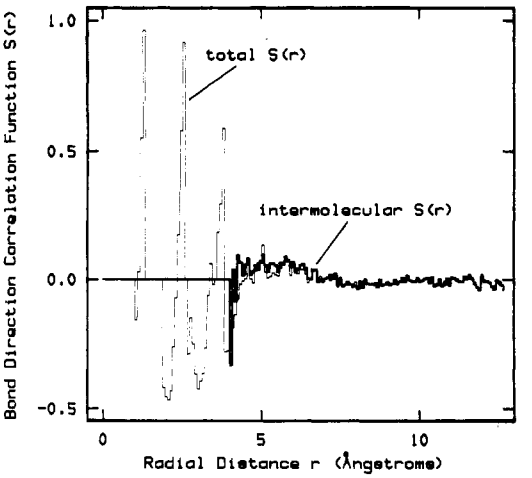

Figure 7. Average bond direction correlation function $S(r)$ in the 15 "relaxed" model systems between skeletal chords with given distance r between their centers. See text for details.

Table V
Group Pair Distribution Functions

pair species $\alpha\beta$	dist r_b, Å	$(4\pi r_b^2/V)A_b$[a]
C-C	1.53	$\frac{2x-2}{(2x-1)(x-1)} = 0.01325$
	2.537	$\frac{x-2}{(2x-1)(x-1)} = 0.00653$
	2.566	$\frac{x-1}{(2x-1)(x-1)} = 0.00662$
C-H	1.10	$\frac{1}{2x-1} = 0.00662$
	2.127	$\frac{2(x-1)}{(3x-2)(2x-1)} = 0.00440$
	2.156	$\frac{4(x-1)}{(3x-2)(2x-1)} = 0.00879$
C-R	1.53	$\frac{1}{2x-1} = 0.00662$
	2.537	$\frac{2x}{(2x-1)(x+2)} = 0.01291$
H-H	1.764	$\frac{2}{3(3x-2)} = 0.00295$
H-R	2.127	$\frac{1}{3x-2} = 0.00442$
R-R	2.537	$\frac{4}{(x+2)(x+1)} = 0.00067$

[a] Fraction of total number of $\alpha\beta$ pairs separated by r_b due to connectivity.

atoms are considered for obtaining $\langle s^2\rangle^{1/2}$), it is also less prone to errors due to limited sample size than $\langle r^2\rangle^{1/2}$. The dimensions of the parent chains are barely distinguishable from those of unperturbed chains; they are slightly smaller. Vactello et al.[16] have reported size and conformation measures obtained from their model of liquid triacontane. It is interesting to note that their chains, too, appear to be somewhat collapsed in comparison to the RIS model predictions.

To explore the *shape* of the parent chains we computed, for each one of them, the eigenvalues $\overline{X^2}$, $\overline{Y^2}$, $\overline{Z^2}$ of the radius of gyration tensor.[35,36] These were used to calculate the shape asphericity[36] $b = \overline{X^2} - {}^1/_2(\overline{Y^2} + \overline{Z^2})$, the acylindricity[36] $c = \overline{Y^2} - \overline{Z^2}$, and the relative anisotropy[36] $\kappa^2 = (b^2$

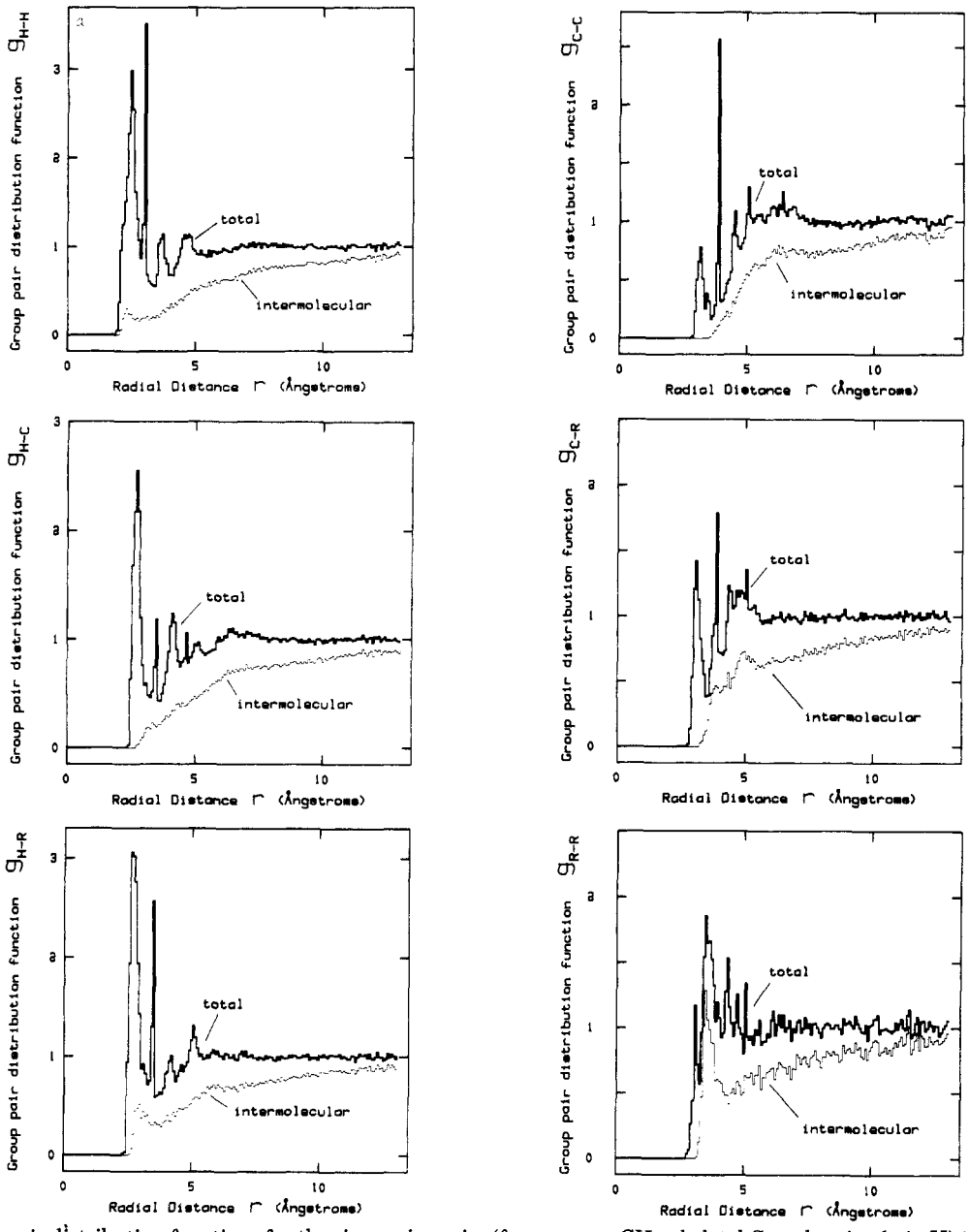

Figure 8. Group pair distribution functions for the six species pairs (from groups CH_3, skeletal C, and main-chain H) in all 15 "relaxed" model structures.

$+ 3c^2/4)/s^4$. Values of the reduced measures $\langle \overline{X^2} \rangle / \langle \overline{Z^2} \rangle$, $\langle \overline{Y^2} \rangle / \langle \overline{Z^2} \rangle$, $\langle b \rangle / \langle s^2 \rangle$, $\langle c \rangle / \langle s^2 \rangle$ and $\langle \kappa^2 \rangle$, obtained by averaging over the ensemble of 15 parent chains, are shown in Table IV. The same measures were computed by Monte Carlo generation of 2000 unperturbed chains (configurations and conformations) with $x = 76$ and $f_m = 0.48$; they are also displayed in Table IV. Excellent agreement between the bulk results and the RIS model predictions is observed; the *shape* of the parent chains is indistinguishable from that of unperturbed coils.

Structure of the Glassy Polymeric Bulk. The model systems obtained in this work provide us with detailed information not only on intramolecular structure but also on the intermolecular aspects, i.e., the relative arrangement of chains in the bulk.

The bond direction correlation function $S(r)$, derived from eq 7 by averaging over chord pairs with given distance r between the chord centers, is plotted in Figure 7 as a thin line. The purely intermolecular part of $S(r)$, obtained by considering those chord pairs only that belong to different images of the parent chain, is also displayed (bold line). The fact that $S(r)$ goes to 0 at large distances proves that there is no long-range correlation; i.e., our model cubes are truly amorphous systems. The sharp correlation pattern observed at short distances is completely intramolecular, i.e., caused by connectivity and conformation along the parent chain. For example, the three maxima at 1.3, 2.5, and 3.8 Å are attributable to t, tt, and ttt conformations.

At the shortest possible intermolecular distances there is a tendency for perpendicular arrangements (perhaps due to the "rough" surface of the chains); at slightly larger distances there is a very weak trend toward parallelism.

The pair distribution functions $g_{\alpha\beta}$ ($\alpha, \beta \in \{H, C, R\}$) for all six species pairs in the systems are shown as bold lines in Figure 8. If V is the volume of a model cube, the function $g_{\alpha\beta}$ is defined so that the quantity $(1/V)(4\pi r^2) g_{\alpha\beta}(r)\, dr$ is equal to the probability of finding an α center and a β center in the distance interval r to $r + dr$. The method of obtaining g from the model is discussed elsewhere.[30] Only pairs whose separation is conformation dependent have been included in Figure 8. Contributions from pairs whose distance is fixed due to connectivity

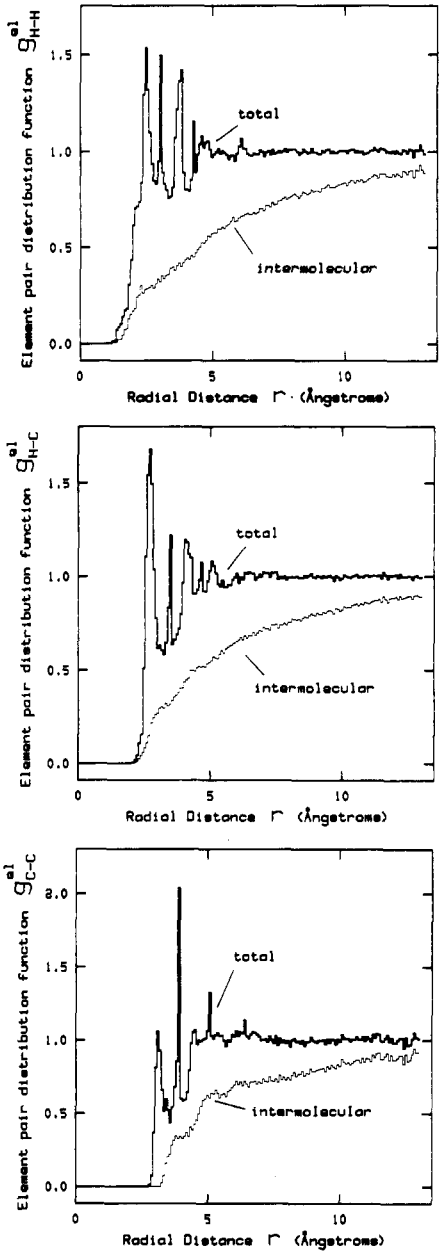

Figure 9. Element pair distribution functions for the three element pairs (from atoms C and H) in all 15 "relaxed" model structures.

would appear as "Dirac pulses" on the plots. The location and magnitude of these pulses are listed in Table V. The distributions of intergroup distances were also calculated for the parent chains and subtracted from the total $g_{\alpha\beta}$'s to obtain the *intermolecular* part of the pair distribution functions, $g_{\alpha\beta}^{\text{inter}}(r)$. The function $g_{\alpha\beta}^{\text{inter}}(r)$ is such that the quantity of $(1/V)(4\pi r^2)g_{\alpha\beta}^{\text{inter}}(r)\,dr$ is equal to the probability of finding an α center and a β center *not* belonging to the same chain and separated by a distance in the interval r to $r + dr$. In Figure 8 the intermolecular parts of the pair distribution functions are displayed as thin lines.

At long distances all pair distribution functions approach unity, indicating that no long-range structure exists (as one would expect from a purely amorphous system). The intermolecular functions $g_{\alpha\beta}^{\text{inter}}$ rise more or less smoothly with increasing distance toward an asymptotic value of one. The sharp correlations observed at small distances in $g_{\alpha\beta}(r)$ are almost entirely intramolecular. The intermolecular pair distribution functions display some subtle structural

Table VI
Element Pair Distribution Functions

pair species $\alpha\beta$	dist r_b, Å	$(4\pi r_b^2/V)A_b$[a]
C-C	1.53	$\frac{2}{3x+1} = 0.00873$
	2.537	$\frac{2}{3x+1} = 0.00873$
	2.566	$\frac{2(x-1)}{3x(3x+1)} = 0.00287$
C-H	1.10	$\frac{1}{3x+1} = 0.00437$
	2.127	$\frac{3x}{(3x+1)(6x+4)} = 0.00216$
	2.156	$\frac{4(x-1)}{(3x+1)(6x+4)} = 0.00285$
	2.168	$\frac{3(x+2)}{(3x+1)(6x+4)} = 0.00222$
	2.759	$\frac{2(x+2)}{(3x+1)(6x+4)} = 0.00148$
	2.813	$\frac{2(x+2)}{(3x+1)(6x+4)} = 0.00148$
	3.486	$\frac{2(x+2)}{(3x+1)(6x+4)} = 0.00148$
H-H	1.764	$\frac{x-1}{(6x+3)(3x+2)} = 0.00071$
	1.790	$\frac{3(x+2)}{(6x+3)(3x+2)} = 0.00222$
	2.457	$\frac{2(x+2)}{(6x+3)(3x+2)} = 0.00148$
	2.524	$\frac{2}{(6x+3)(3x+2)} = 0.00002$
	2.643	$\frac{2}{(6x+3)(3x+2)} = 0.00002$
	3.050	$\frac{x+2}{(6x+3)(3x+2)} = 0.00074$
	3.143	$\frac{4}{(6x+3)(3x+2)} = 0.00004$
	3.755	$\frac{4}{(6x+3)(3x+2)} = 0.00004$
	3.822	$\frac{4}{(6x+3)(3x+2)} = 0.00004$
	4.315	$\frac{2}{(6x+3)(3x+2)} = 0.00002$

[a] Fraction of $\alpha\beta$ pairs separated by r_b due to connectivity.

features, but beyond 10 Å there is essentially no intermolecular correlation; only the HH, HR, and RR (i.e., the substituent–substituent; R stands for methyl) distributions display a well-defined maximum at a distance roughly equal to the sum of the van der Waals radii of the species involved. This "first coordination shell" appears particularly pronounced in the RR case. (The high noise level in this case is due to the small number of methyl substituents in the system.) Skeletal carbons of different chains are kept apart by the substituents surrounding them, so that the principal feature of the carbon–carbon intermolecular distribution is a broad hump in the vicinity of 6.3 Å. The C–R intermolecular distribution displays two humps around 3.9 Å (first coordination shell) and 5 Å. Broad

humps of intermolecular origin at distances beyond 5 Å can also be discerned in the H–C and H–R distributions.

Note that the pair distribution functions have been calculated from a static ensemble of structures. In reality thermal motion will tend to broaden the peaks and to reduce their height.

Vacatello et al.[16] present a methylene–methylene pair distribution function, based on their model of liquid triacontane, which is qualitatively very similar to our skeletal carbon–carbon distribution (see Figure 8). The location and interpretation of the three first intramolecular maxima in our systems is practically identical with theirs, and our g_{CC}^{inter} confirms the presence of some intermolecular contribution in the region around 6.30 Å.

In reality there are no R groups, but only H and C atoms, whose spatial arrangement is characterized by the three element pair distribution functions g_{HH}^{el}, g_{HC}^{el}, and g_{CC}^{el}. To obtain these, we "resolved" each of the methyl groups into a carbon, at the end of the carbon–methyl bond, and three hydrogens, symmetrically bonded to this carbon by bonds of length l_H at an angle of 110° with the methyl stem. All methyls were taken in a staggered conformation with respect to the backbone. The element pair distributions were computed in exactly the same way as the group pair distributions presented above, and are displayed as bold lines in Figure 9. Also shown are the purely intermolecular contributions (thin lines). Again chain connectivity introduces additional "Dirac spikes"; their location and magnitude are listed in Table VI.

Our ensemble of 15 equilibrium structures is currently used to predict the elastic constants of glassy amorphous polypropylene by simulating mechanical deformation of various types and degrees. The element pair distributions are being used to predict X-ray and neutron scattering curves and thus provide a further test of the model structures against experiment. Results will be reported in subsequent publications.

Acknowledgment. We gratefully acknowledge support by NSF Grant No. DMR-8312694 (Polymers Program) and the Texaco–Mangelsdorf Associate Professorship at the Massachusetts Institute of Technology. We also thank Professors Robert E. Cohen and Ioannis V. Yannas for vigorous and helpful discussions.

Appendix 1. Total Potential Energy Function and Its Derivatives

Consider the parent chain and number its skeletal groups from 0 to $2x$. Groups 0 and $2x$ are the terminal methyls; groups $2i - 1$, $1 \le i \le x$, are of the type –CHR–, while groups $2i$, $1 \le i \le x - 1$, are of the type $-CH_2-$. Skeletal bonds are numbered from 1 to $2x$, so that bond i connects groups $i - 1$ and i. The bond rotation angle ϕ_i is the dihedral angle between the planes of bonds $(i - 1, i)$ and bonds $(i, i + 1)$, measured in a right-hand sense relative to trans.[28] The skeletal carbon i is denoted by C_i.

Local reference frames are introduced at skeletal bonds following the conventions of Flory (p 20 of ref 28). The cube ("external") frame of reference, with respect to which all coordinates are ultimately expressed, is denoted as xyz. Eulerian angle ψ_1 is taken as the angle between the x direction and the projection of bond 1 on the xy plane; Eulerian angle ψ_2 is taken as the angle between the z direction and bond 1; Eulerian angle ψ_3 is taken as the dihedral angle between the planes (z direction, bond 1) and (bond 1, bond 2). The coordinates of an atom with respect to the cube frame of reference are denoted by $\mathbf{r}$. The coordinates of the chain start (terminal methyl 0) are denoted by $\mathbf{r}_0$. For any atom in the cube, let j symbolize the index of the skeletal group to which the parent image of this atom is connected.

The position vector $\mathbf{r}$ of an atom in the cube can be expressed in terms of the variables $(\mathbf{r}_0, \psi_1, \psi_2, \psi_3, \phi_2, ..., \phi_{2x-1})$ as (in *matrix notation*)

$$\mathbf{r} = \mathbf{r}_0 + \mathbf{T}_0\mathbf{l} + \mathbf{T}_0\mathbf{T}_1\mathbf{l} + ... + \mathbf{T}_0\mathbf{T}_1 ... \mathbf{T}_{j-1}\mathbf{v}^{(j)} + \lambda\mathbf{a}_x + \mu\mathbf{a}_y + \nu\mathbf{a}_z \quad (A.1)$$

where

$$\mathbf{T}_0 = \begin{bmatrix} \cos\psi_1 \sin\psi_2 & -\cos\psi_1 \cos\psi_2 \cos\psi_3 - \sin\psi_1 \sin\psi_3 & -\cos\psi_1 \cos\psi_2 \sin\psi_3 + \sin\psi_1 \sin\psi_3 \\ \sin\psi_1 \sin\psi_2 & -\sin\psi_1 \cos\psi_2 \cos\psi_3 + \cos\psi_1 \sin\psi_3 & -\sin\psi_1 \cos\psi_2 \sin\psi_3 - \cos\psi_1 \cos\psi_3 \\ \cos\psi_2 & \sin\psi_2 \cos\psi_3 & \sin\psi_2 \sin\psi_3 \end{bmatrix} \quad (A.2)$$

is the orthogonal transformation matrix of "internal" to "external" coordinates,

$$\mathbf{T}_i = \begin{bmatrix} \cos\theta_i & \sin\theta_i & 0 \\ \sin\theta_i \cos\phi_i & -\cos\theta_i \cos\phi_i & \sin\phi_i \\ \sin\theta_i \sin\phi_i & -\cos\theta_i \sin\phi_i & -\cos\phi_i \end{bmatrix} \quad (A.3)$$

$$(i = 1, 2, ..., 2x - 1)$$

is the orthogonal transformation matrix from the reference frame of bond $(i + 1)$ to the reference frame of bond i (by definition, $\phi_1 = 0$), and (from here on we use *vector notation*)

$$\mathbf{l} = l(1, \quad 0, \quad 0) \quad (A.4)$$

$\mathbf{v}^{(j)}$ is the coordinate vector of the parent image in the reference frame of bond j. The possible values of $\mathbf{v}^{(j)}$ are

$$\mathbf{v}^{(j)} = l(1, \quad 0, \quad 0) \quad (A.5a)$$

for a skeletal carbon,

$$\mathbf{v}^{(j)} = l_H\left(-\cos\theta'_H, \quad \cos\theta'_H \cot\frac{\theta'}{2}, \quad \mp\left[1 - \frac{\cos^2\theta'_H}{\sin^2\frac{\theta'}{2}} \right]^{1/2} \right) \quad (A.5b)$$

for a hydrogen attached to an achiral skeletal carbon (the $\mp$ sign distinguishes between the two hydrogen atoms in the methylene group),

$$\mathbf{v}^{(j)} = l_H\left(-\cos\theta''_H, \quad \cos\theta''_H \cot\frac{\theta''}{2}, \quad \pm\left[1 - \frac{\cos^2\theta''_H}{\sin^2\frac{\theta''}{2}} \right]^{1/2} \right) \quad (A.5c)$$

for a hydrogen attached to a chiral skeletal carbon (the $\pm$ sign denotes the chirality), and

$$\mathbf{v}^{(j)} = l_R\left(-\cos\theta''_R, \quad \cos\theta''_R \cot\frac{\theta''}{2}, \quad \mp\left[1 - \frac{\cos^2\theta''_R}{\sin^2\frac{\theta''}{2}} \right]^{1/2} \right) \quad (A.5d)$$

for a methyl substituent (the $\mp$ sign denotes the chirality).

The last three terms in eq A.1 arise from the periodicity of the system: $\mathbf{a}_x$, $\mathbf{a}_y$, and $\mathbf{a}_z$ are the edge vectors of the cube (hereafter called "continuation vectors") while the integers λ, μ, and ν (hereafter called "continuation coefficients") measure the magnitude of the translations required to reach the considered atom of the cube from its image belonging to the parent chain starting at $\mathbf{r}_0$.

By differentiation of eq A.1 one obtains the derivatives of $\mathbf{r}$ with respect to each of the $2x + 1$ degrees of freedom:

$$\frac{\partial \mathbf{r}}{\partial \psi} = \mathbf{v}_\psi \times \{\mathbf{r} - \mathbf{r}_0 - \lambda \mathbf{a}_x - \mu \mathbf{a}_y - \nu \mathbf{a}_z\} \tag{A.6}$$

where $\psi \in \{\psi_1, \psi_2, \psi_3\}$ and

$$\text{for } \psi = \psi_1 \qquad \mathbf{v}_\psi = (0, \quad 0, \quad 1) \tag{A.7a}$$

$$\text{for } \psi = \psi_2 \qquad \mathbf{v}_\psi = (-\sin \psi_1, \quad \cos \psi_1, \quad 0) \tag{A.7b}$$

$$\text{for } \psi = \psi_3 \qquad \mathbf{v}_\psi = (-\cos \psi_1 \sin \psi_2, \quad -\sin \psi_1 \sin \psi_2, \quad -\cos \psi_2) \tag{A.7c}$$

$$\frac{\partial \mathbf{r}}{\partial \phi_i} = \mathbf{0}, \quad \text{if } j < i \tag{A.8a}$$

$$\frac{\partial \mathbf{r}}{\partial \phi_i} = \frac{1}{l}[\mathbf{r}_{c_i} - \mathbf{r}_{c_{i-1}} - (\lambda_{c_i} - \lambda_{c_{i-1}})\mathbf{a}_x - (\mu_{c_i} - \mu_{c_{i-1}})\mathbf{a}_y - (\nu_{c_i} - \nu_{c_{i-1}})\mathbf{a}_z] \times [\mathbf{r} - \mathbf{r}_{c_i} - (\lambda - \lambda_{c_i})\mathbf{a}_x - (\mu - \mu_{c_i})\mathbf{a}_y - (\nu - \nu_{c_i})\mathbf{a}_z], \quad \text{if } i < j \tag{A.8b}$$

The derivatives of all interatomic distances can now be found. In particular, for the distance $|\mathbf{r}_1 - \mathbf{r}_{2,m}|$ between an atom, 1, and the image of another atom, 2, that lies closest to 1, one obtains

$$\frac{\partial(\mathbf{r}_1 - \mathbf{r}_{2,m})}{\partial \psi} = -\mathbf{v}_\psi \cdot \{(\lambda_1 - \lambda_{2,m})\mathbf{a}_x + (\mu_1 - \mu_{2,m})\mathbf{a}_y + (\nu_1 - \nu_{2,m})\mathbf{a}_z\} \times \frac{\mathbf{r}_1 - \mathbf{r}_{2,m}}{|\mathbf{r}_1 - \mathbf{r}_{2,m}|} \tag{A.9}$$

and

$$\frac{\partial}{\partial \phi_i}|\mathbf{r}_1 - \mathbf{r}_{2,m}| = 0, \qquad \text{for } j_1 < i \tag{A.10a}$$

$$\frac{\partial}{\partial \phi_i}|\mathbf{r}_1 - \mathbf{r}_{2,m}| = -\frac{\mathbf{r}_{c_i} - \mathbf{r}_{c_{i-1}} - (\lambda_{c_i} - \lambda_{c_{i-1}})\mathbf{a}_x - (\mu_{c_i} - \mu_{c_{i-1}})\mathbf{a}_y - (\nu_{c_i} - \nu_{c_{i-1}})\mathbf{a}_z}{|\mathbf{r}_1 - \mathbf{r}_{2,m}|l} \cdot (\mathbf{r}_1 - \mathbf{r}_{2,m}) \times [\mathbf{r}_1 - \mathbf{r}_{c_i} - (\lambda_1 - \lambda_{c_i})\mathbf{a}_x - (\mu_1 - \mu_{c_i})\mathbf{a}_y - (\nu_1 - \nu_{c_i})\mathbf{a}_z], \qquad \text{for } j_2 < i \le j_1 \tag{A.10b}$$

$$\frac{\partial}{\partial \phi_i}|\mathbf{r}_1 - \mathbf{r}_{2,m}| = \frac{\mathbf{r}_{c_i} - \mathbf{r}_{c_{i-1}} - (\lambda_{c_i} - \lambda_{c_{i-1}})\mathbf{a}_x - (\mu_{c_i} - \mu_{c_{i-1}})\mathbf{a}_y - (\nu_{c_i} - \nu_{c_{i-1}})\mathbf{a}_z}{|\mathbf{r}_1 - \mathbf{r}_{2,m}|l} \cdot (\mathbf{r}_1 - \mathbf{r}_{2,m}) \times [(\lambda_{2,m} - \lambda_1)\mathbf{a}_x + (\mu_{2,m} - \mu_1)\mathbf{a}_y + (\nu_{2,m} - \nu_1)\mathbf{a}_z], \qquad \text{for } i \le j_2 \tag{A.10c}$$

The total potential energy function is the sum

$$U(\psi,\phi) = \sum_{\substack{i,\ \text{bonds of} \\ \text{parent chain} \\ 2 \le i \le 2x-1}} U_\phi(\phi_i) + \sum_{\substack{1,\ \text{atoms} \\ \text{in cube} \\ j_1 > 0}} \sum_{\substack{2,\ \text{atoms} \\ \text{in cube} \\ 0 \le j_2 < j_1}} U^{NB}(|\mathbf{r}_1 - \mathbf{r}_{2,m}|) \tag{A.11}$$

where the functions $U_\phi(\phi)$ and $U^{NB}(r)$ have been introduced in the main text. The double summation runs over atom pairs whose parent images are at least three bonds apart, so that their distance is conformation dependent. The derivatives of U with respect to the degrees of freedom are obtained by direct differentiation of eq A.11 and use of eq A.9 and A.10.

Introducing the abbreviated notations

$$\mathbf{b}_i = \mathbf{r}_{c_i} - \mathbf{r}_{c_{i-1}} - (\lambda_{c_i} - \lambda_{c_{i-1}})\mathbf{a}_x - (\mu_{c_i} - \mu_{c_{i-1}})\mathbf{a}_y - (\nu_{c_i} - \nu_{c_{i-1}})\mathbf{a}_z \tag{A.12a}$$

$$\mathbf{r}_{1i} = \mathbf{r}_1 - \mathbf{r}_{c_i} - (\lambda_1 - \lambda_{c_i})\mathbf{a}_x - (\mu_1 - \mu_{c_i})\mathbf{a}_y - (\nu_1 - \nu_{c_i})\mathbf{a}_z \tag{A.12b}$$

$$\mathbf{r}_{12} = \mathbf{r}_1 - \mathbf{r}_2 - (\lambda_1 - \lambda_2)\mathbf{a}_x - (\mu_1 - \mu_2)\mathbf{a}_y - (\nu_1 - \nu_2)\mathbf{a}_z \tag{A.12c}$$

$$\mathbf{r}_m = \mathbf{r}_1 - \mathbf{r}_{2,m}; \qquad r_m = |\mathbf{r}_m| \tag{A.12d}$$

$$\mathbf{a}_{12} = (\lambda_{2,m} - \lambda_1)\mathbf{a}_x + (\mu_{2,m} - \mu_1)\mathbf{a}_y + (\nu_{2,m} - \nu_1)\mathbf{a}_z = \mathbf{r}_{12} - \mathbf{r}_m \tag{A.12e}$$

$$\mathbf{r}_{2i,m} = \mathbf{r}_{2,m} - \mathbf{r}_{c_i} - (\lambda_1 - \lambda_{c_i})\mathbf{a}_x - (\mu_1 - \mu_{c_i})\mathbf{a}_y - (\nu_1 - \nu_{c_i})\mathbf{a}_z = \mathbf{r}_{1i} - \mathbf{r}_m \tag{A.12f}$$

$$U'_{12} = \left.\frac{\partial U^{NB}}{\partial r}\right|_{r=r_m}; \qquad U''_{12} = \left.\frac{\partial^2 U^{NB}}{\partial r^2}\right|_{r=r_m}; \qquad U'_\phi = \frac{\partial U_\phi}{\partial \phi}; \qquad U''_\phi = \frac{\partial^2 U_\phi}{\partial \phi^2} \tag{A.12g}$$

we obtain

Gradient

$$\frac{\partial U}{\partial \psi} = \sum_{j_1 > 0} \sum_{0 \le j_2 < j_1} \frac{U'_{12}}{r_m} \mathbf{v}_\psi \cdot (\mathbf{a}_{12} \times \mathbf{r}_m) \tag{A.13}$$

$$\frac{\partial U}{\partial \phi_i} = U'_\phi(\phi_i) + \frac{1}{l}\left[\sum_{j_1 \ge i} \sum_{0 \le j_2 < i} \frac{U'_{12}}{r_m} \mathbf{b}_i \cdot (\mathbf{r}_{1i} \times \mathbf{r}_m) + \sum_{j_1 > i} \sum_{i \le j_2 < j_1} \frac{U'_{12}}{r_m} \mathbf{b}_i \cdot (\mathbf{a}_{12} \times \mathbf{r}_m)\right] \tag{A.14}$$

Hessian

$$\frac{\partial^2 U}{\partial \psi_i \partial \psi_k} = \frac{1}{l} \sum_{j_1 \ge 0} \sum_{0 \le j_2 < j_1} \left\{\frac{1}{r_m^2}\left(U''_{12} - \frac{U'_{12}}{r_m}\right) \times [\mathbf{v}_{\psi_k} \cdot (\mathbf{a}_{12} \times \mathbf{r}_m)][\mathbf{v}_{\psi_i} \cdot (\mathbf{a}_{12} \times \mathbf{r}_m)] + \frac{U'_{12}}{r_m}[(\mathbf{v}_{\psi_k} \cdot \mathbf{v}_{\psi_i})(\mathbf{r}_{12} \cdot \mathbf{a}_{12}) - (\mathbf{v}_{\psi_k} \cdot \mathbf{r}_{12})(\mathbf{v}_{\psi_i} \cdot \mathbf{a}_{12})]\right\} \qquad \text{with } (i, k) \in \{1, 2, 3\}^2, \quad i > k \tag{A.15}$$

$$\frac{\partial^2 U}{\partial \psi \partial \phi_i} = \frac{1}{l}\left[\sum_{j_1 \ge i} \sum_{0 \le j_2 < i} \left\{\frac{1}{r_m^2}\left(U''_{12} - \frac{U'_{12}}{r_m}\right)[\mathbf{v}_\psi \cdot (\mathbf{a}_{12} \times \mathbf{r}_m)][\mathbf{b}_i \cdot (\mathbf{r}_{1i} \times \mathbf{r}_m)] + \frac{U'_{12}}{r_m}[(\mathbf{b}_i \cdot \mathbf{v}_\psi)(\mathbf{r}_{1i} \cdot \mathbf{a}_{12}) - (\mathbf{v}_\psi \cdot \mathbf{r}_{1i})(\mathbf{b}_i \cdot \mathbf{a}_{12})]\right\} + \sum_{j_1 \ge i} \sum_{i \le j_2 < j_1} \left\{\frac{1}{r_m^2}\left(U''_{12} - \frac{U'_{12}}{r_m}\right)[\mathbf{v}_\psi \cdot (\mathbf{a}_{12} \times \mathbf{r}_m)][\mathbf{b}_i \cdot (\mathbf{a}_{12} \times \mathbf{r}_m)] + \frac{U'_{12}}{r_m}[(\mathbf{b}_i \cdot \mathbf{v}_\psi)(\mathbf{r}_{12} \cdot \mathbf{a}_{12}) - (\mathbf{b}_i \cdot \mathbf{a}_{12})(\mathbf{v}_\psi \cdot \mathbf{r}_{12})]\right\}\right] \tag{A.16}$$

$$\frac{\partial^2 U}{\partial\phi_i\partial\phi_k} = \delta_{ik}U''_{\phi}(\phi_i) + \frac{1}{l}\Bigg[\sum_{\substack{1\\ j_1\geq i}}\sum_{\substack{2\\ 0\leq j_2<k}}\Bigg\{\frac{1}{r_m^2}\times \left(U''_{12} - \frac{U'_{12}}{r_m}\right)[\mathbf{b}_k\cdot(\mathbf{r}_{1k}\times\mathbf{r}_m)][\mathbf{b}_i\cdot(\mathbf{r}_{1i}\times\mathbf{r}_m)] + \frac{U'_{12}}{r_m}[(\mathbf{b}_i\cdot\mathbf{b}_k)(\mathbf{r}_{1i}\cdot\mathbf{r}_{2k,m}) - (\mathbf{b}_i\cdot\mathbf{r}_{2k,m})(\mathbf{b}_k\cdot\mathbf{r}_{1i})]\Bigg\} + \sum_{\substack{1\\ j_1\geq i}}\sum_{\substack{2\\ k\leq j_2<i}}\Bigg\{\frac{1}{r_m^2}\left(U''_{12} - \frac{U'_{12}}{r_m}\right)\times [\mathbf{b}_k\cdot(\mathbf{a}_{12}\times\mathbf{r}_m)][\mathbf{b}_i\cdot(\mathbf{r}_{1i}\times\mathbf{r}_m)] + \frac{U'_{12}}{r_m}[(\mathbf{b}_i\cdot\mathbf{b}_k)(\mathbf{r}_{1i}\cdot\mathbf{a}_{12}) - (\mathbf{b}_i\cdot\mathbf{a}_{12})(\mathbf{b}_k\cdot\mathbf{r}_{1i})]\Bigg\} + \sum_{\substack{1\\ j_1>i}}\sum_{\substack{2\\ i\leq j_2<j_1}}\Bigg\{\frac{1}{r_m^2}\left(U''_{12} - \frac{U'_{12}}{r_m}\right)[\mathbf{b}_k\cdot(\mathbf{a}_{12}\times\mathbf{r}_m)]\times [\mathbf{b}_i\cdot(\mathbf{a}_{12}\times\mathbf{r}_m)] + \frac{U'_{12}}{r_m}[(\mathbf{b}_i\cdot\mathbf{b}_k)(\mathbf{r}_{12}\cdot\mathbf{a}_{12}) - (\mathbf{b}_i\cdot\mathbf{a}_{12})(\mathbf{b}_k\cdot\mathbf{r}_{12})]\Bigg\}\Bigg] \quad \text{with } i \geq k \quad \text{(A.17)}$$

where δ_{ik} is the Kronecker δ function.

Appendix 2. Bonded Contributions to the Pair Distribution Functions

The bonded group pair distribution functions and the bonded element pair distribution functions are given in Tables V and VI, respectively. In those tables r_b symbolizes the location of each "Dirac pulse" on the r axis (in Å), A_b symbolizes the area of the "Dirac pulse" in a $g(r)$ plot (in Å), and V is the cube volume (in Å^3).

Registry No. Polypropylene (homopolymer), 9003-07-0.

References and Notes

(1) Cohen, M. H.; Grest, G. S. *Ann. N.Y. Acad. Sci.* **1981**, *371*, 199–209.
(2) Kirste, R. G.; Kruse, W. A.; Schelten, J. *Makromol. Chem.* **1973**, *162*, 299–303.
(3) Cotton, J. P.; Farnoux, B.; Jannink, G.; Mous, J.; Picot, C. *C.R. Hebd. Seances Acad. Sci., Ser. C* **1972**, *275*, 175–178.
(4) Ballard, D. G.; Wignall, G. D.; Schelten, J. *Eur. Polym. J.* **1973**, *9*, 965–969.
(5) Hayashi, H.; Flory, P. J. *Macromolecules* **1983**, *16*, 1328–1335.
(6) Flory, P. J. "Principles of Polymer Chemistry"; Cornell University Press: Ithaca, NY, 1953; p 602.
(7) Pechhold, W.; Liska, E.; Grossmann, H. P.; Hägele, P. C. *Pure Appl. Chem.* **1976**, *46*, 127–134.
(8) Alexandrowicz, Z.; Accad, Y. *J. Chem. Phys.* **1971**, *54*, 5338–5345.
(9) De Vos, E.; Bellemans, A. *Macromolecules* **1974**, *7*, 812–814.
(10) de Santis, R.; Zachmann, H. G. *Colloid Polym. Sci.* **1977**, *255*, 729–734.
(11) Skvortsov, A. M.; Sariban, A. A.; Birshtein, T. M. *Vysokomol. Soedin.* **1977**, *5*, 1014–1021.
(12) Jagodic, F.; Borštnik, B.; Ažman, A. *Makromol. Chem.* **1973**, *173*, 221–231.
(13) de Santis, R.; Zachmann, H. G. *Prog. Colloid Polym. Sci.* **1978**, *64*, 281–285.
(14) Wall, F. T.; Seitz, W. A. *J. Chem. Phys.* **1977**, *67*, 3722–3726.
(15) Bishop, M.; Ceperley, D.; Frisch, H. L.; Kalos, M. H. *J. Chem. Phys.* **1980**, *72*, 3228–3235.
(16) Vacatello, M.; Avitabile, G.; Corradini, P.; Tuzi, A. *J. Chem. Phys.* **1980**, *73*, 543–552.
(17) Weber, T. A.; Helfand, E. *J. Chem. Phys.* **1979**, *71*, 4760–4762.
(18) Bovey, F. A.; Winslow, F. H., Eds. "Macromolecules: An Introduction to Polymer Science"; Academic Press: New York, 1979; p 8.
(19) Brandrup, J.; Immergut, E. H., Eds. "Polymer Handbook", 2nd ed.; Wiley Interscience: New York, 1975; p V-23.
(20) Kaufmann, H. S.; Falcetta, J. J. "Introduction to Polymer Science and Technology"; Wiley: New York, 1977; p 244 and 294.
(21) Suter, U. W. *Macromolecules* **1981**, *14*, 523–528. Suter, U. W.; Neuenschwander, P. *Macromolecules* **1980**, *14*, 528–532.
(22) Bondi, A. "Physical Properties of Molecular Crystals, Liquids and Glasses"; Wiley: New York, 1968; p 387.
(23) Van Krevelen, D. W.; Hoftyzer, P. J. "Properties of Polymers—Their Estimation and Correlation with Chemical Structure"; Elsevier: New York, 1976, pp 130, 137, and 275.
(24) Uhlmann, D. R.; Kreidl, N. J., Eds. "Glass Science and Technology"; Academic Press: New York, 1983; Vol. I, p 6.
(25) Maeda, K.; Takeuchi, S. *Philos. Mag. A* **1981**, *44*, 643–656.
(26) Egami, T.; Maeda, K.; Vitek, V. *Philos. Mag. A* **1980**, *41*, 883–901.
(27) Suter, U. W.; Flory, P. J. *Macromolecules* **1975**, *8*, 765–776.
(28) Flory, P. J. "Statistical Mechanics of Chain Molecules"; Wiley-Interscience: New York, 1969; Chapters I and III.
(29) Flory, P. J. *Macromolecules* **1974**, *7*, 381–392.
(30) Theodorou, D. N.; Suter, U. W. *J. Chem. Phys.* **1985**, *82*, 955–966.
(31) Dennis, J. E.; Moré, J. J. *SIAM Rev.* **1977**, *19*, 46–89.
(32) Hillstrom, K. "Nonlinear Optimization Routines in AMDLIB", Technical Memorandum No. 297, Argonne National Laboratory, Applied Mathematics Division, 1976; Subroutine GQBFGS in AMDLIB, 1976, Argonne, IL.
(33) Exploratory calculations, not reported here, have shown that, for a system with $x = 76$, the computation of the gradient would be 17 times slower with a finite-difference scheme than with out analytical expressions (see Appendix 1).
(34) Dill, K. A.; Flory, P. J. *Proc. Natl. Acad. Sci. U.S.A.* **1980**, *77*, 3115–3119.
(35) Šolc, K.; Stockmayer, W. H. *J. Chem. Phys.* **1971**, *54*, 2756–2757. Šolc, K. *J. Chem. Phys.* **1971**, *55*, 335–344.
(36) Theodorou, D. N.; Suter, U. W. *Macromolecules* **1985**, *18*, 1206–1214.